Ref. Ares(2025)3516634 - 30/04/2025

Tech UPGRADE

D2.3 First/final reactors’ heat and mass transfer results

Funded by the European Union

This project has received funding from European Union’s Horizon Europe’s Research and Innovation Program under grant agreement No. 101103966. Views and opinions expressed are however those of the author(s) only and do not necessarily reflect those of the European Union or the European Climate, Infrastructure and Environment Executive Agency (CINEA). Neither the European Union nor the granting authority can be held responsible for them.

Deliverable 2.3

Actual Submission Date:	**30/04/2025**
Produced by:	**UT- Roushenas, Ramin**

TechUPGRADE

techupgrade.eu

HORIZON-CL5-2022-D4-01

Thermochemical Heat Recovery and Upgrade for Industrial Processes

Grant Agreement no.: 101103966

Start date of project: 1 May 2023 - Duration: 48 months

DELIVERABLE FACTSHEET

Deliverable D2.3	
Nature of the Deliverable:	R— Document, report
Due date of the Deliverable:	M24 – 30/04/2025
Actual Submission Date:	M24 – 30/04/2025
Produced by:	Ramin Roushenas
Contributors:	Marco Ballatore, Singh K. Abhishek
Work Package Leader	UT – Singh Abhishek
Reviewed by:	DTU- Hamid Reza Rahbari

Dissemination level	
X	PU = Public
	PP = Restricted to other programme participants (including the EC)
	RE = Restricted to a group of the consortium (including the EC)
	CO = Confidential, only members of the consortium (including the EC)

Contents

Figures

1 Summary

This deliverable describes the numerical model created for the simulation of the thermochemical heat upgrade reactor. The design of this reactor was described in deliverable 2.1. This model is used to predict the behaviour of the reactor operation in both hydration and dehydration modes, such as changes in hydration levels, temperature, flow within the reactor, etc. This reactor is also fabricated and tested at DLR. Strontium Bromide is used as a reactive material, and the experimental data were used to perform the numerical model validation. The model shows a good agreement with the experimental results during the hydration process, which is not the case during the dehydration process. This discrepancy could be because of uncertainty in the volume change of the reactive material within the reactor and the heat losses from the reactor boundaries during this process. The model will be further validated using the experimental data from the next version of the reactor.

2 Introduction

In Thermochemical Heat Transformers (TCHT), salt hydrate acts as a reactive material that undergoes dehydration through the low-temperature heat and stores it chemically by breaking bonds. The hydration process can take place by the recombination of water vapor and salt ($Salt.xH_2O_{(s)} + \Delta H \rightleftharpoons (x-y)Salt_{(s)} + yH_2O_{(g)}$). The temperature of the material in this reaction depends on the pressure of water vapor according to the Van't Hoff equation. A higher vapor pressure, generated using solar heat/industrial waste heat, leads to a greater temperature boost, thereby providing a flexible output temperature for industrial requirements. The performance of a packed bed reactor, which operates in a closed system configuration, is limited by the rate of heat being extracted from the TCM due to material's poor thermal conductivity along with the limited contact surface of the HTF and the TCM. So, to face these issues, not only selection of heat exchanger type (i.e., among shell and tube, plate, etc.) is important, but also investigating promising solutions to maximize the proposed reactor performance is essential.

Focusing on the modeling perspective, several studies have developed numerical models to enhance the understanding and prediction of thermochemical energy storage systems. Stengler et al. [1] formulated a finite element method (FEM) model to simulate a gas-solid thermochemical storage system utilizing strontium bromide. Their simulations revealed that the heat transfer coefficient between the reactive bulk material and the heat exchanger surface plays a crucial role in determining the system's thermal power output. Humbert and Sciacovelli [2] proposed a topology optimization framework to design heat transfer enhancement structures in closed thermochemical energy storage reactors. Their model combined heat and mass transfer equations with time-dependent objective functions. The generated designs achieved up to 286% higher performance compared to conventional fin designs, demonstrating that topology optimization can discover novel configurations beyond traditional parametric methods. Li et al. [3] integrated experimental characterization with numerical modeling to evaluate the performance of a $LiOH \cdot H_2O$/expanded graphite composite sorbent. By deriving kinetic parameters experimentally and incorporating them into a simulation of the storage unit, they analyzed the coupled heat and mass transfer behavior. The numerical results indicated a thermal power output of 123 W and a thermal efficiency of 83.6%, supporting the composite's effectiveness for low-grade thermal energy storage. Rui et al. [4] developed a model to optimize a novel salt hydrate-based reactor. Using COMSOL Multiphysics, they coupled transport phenomena with reaction kinetics under local thermodynamic equilibrium assumptions. The model, validated against experimental data, highlighted inlet air temperature as the most influential factor on reactor performance. Their optimized design features an extended air outlet channel, improved thermal efficiency, and shortened reaction time. In the present research, a COMSOL-based Multiphysics model was developed to understand the heat and mass transfer within the TechUPGRADE reactor.

3 Simulation

A COMSOL-based numerical model of the reactor is developed to evaluate the performance of the proposed reactor. The reactor's behavior during both the hydration and dehydration processes was analyzed using transient simulations.

3.1 Domains and Assumptions

Due to the complex geometry of the reactor, a 3D model was employed to achieve higher accuracy compared to a 2D representation. The reactor geometry with multiple domains, including the reactive material, fiberglass, metal mesh, heat exchanger, heat transfer fluid (HTF) path, and interior pipes, based on the actual dimensions of the experimental setup, is shown in Figure 1.

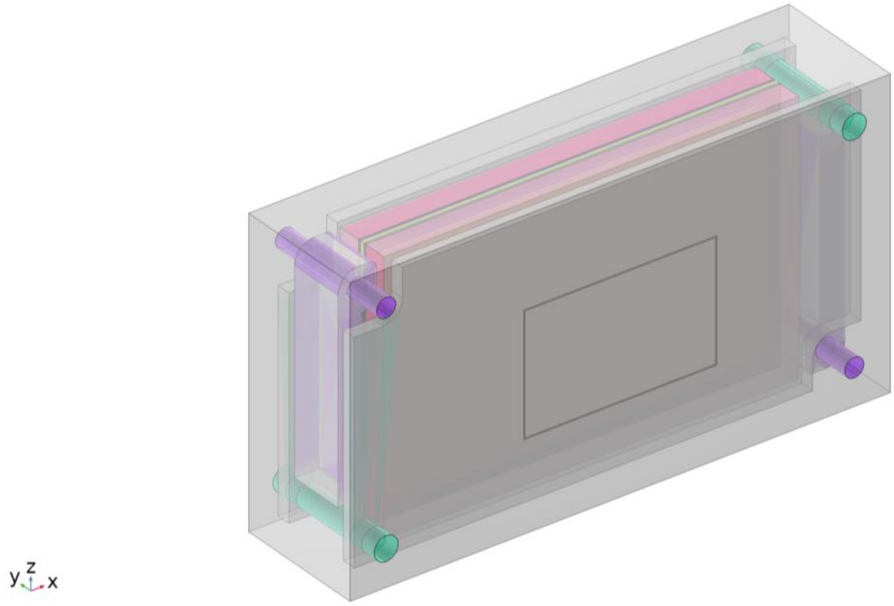

Figure 1. Reactor components

During the experiments, the bottom of the reactor was insulated, while the remaining surfaces were maintained at a constant temperature using heating cords. However, temperature measurements within the lower bed indicated noticeable heat loss. To ensure the validity of the numerical model, these experimental conditions were replicated in the simulation; thus, to estimate heat loss from the reactor, a preheating phase was simulated, accounting for convective losses from all external surfaces except the insulated bottom. A transient simulation is applied to the solver. The changes in pressure during experiments were applied as boundary conditions. On the other hand, the reactor was not leak-tight during experiments, and heating cords supplied the required heat. Therefore, the boundary conditions of the simulation follow the same conditions. Also, the radiation heat transfer is negligible since the reactor operates at low temperatures.

3.2 Governing equations

Reaction kinetics

To predict the rates at which the chemical reactions take place, the following equations are solved for dehydration and hydration reactions, respectively [5]:

$$\frac{\partial X}{\partial t} = 1.38 \times 10^{6} exp\left(\frac{E_a}{RT}\right)(1 - X)\left(1 - \frac{p}{p_{eq,dhyd}}\right)^{1.79} \tag{1}$$

$$\frac{\partial X}{\partial t} = 3.04 \times 10^{-5}(1 - X)\left(T|_{P_{eq,hyd}} - T\right)^{1.79} \tag{2}$$

where X represents the extent of reaction. E_a is activation energy, R is universal gas constant, T is the temperature and p is the pressure. Also, equilibrium pressures are related to the temperature by:

$$log\left(p_{eq,hyd}\right) = 8.18 - \frac{3.19 \times 10^3}{T} \tag{3}$$

$$log\left(p_{eq,dhyd}\right) = 14.69 - \frac{6.41 \times 10^3}{T} \tag{4}$$

Mass conservation

Because the bed takes up and releases steam during hydration and dehydration, a mass source term is introduced within the porous reactive material, linked to the reaction kinetics. The mass balance for the compressible reactive gas (steam) is expressed as follows:

$$\frac{\partial(\varepsilon\rho_g)}{\partial t} + \nabla.\left(\rho_g \vec{v}\right) = \frac{dX}{dt}\varphi M_{H_2O} \tag{5}$$

where ε is the porosity at a specific time of calculations,ρ_g is the density of gas, $\vec{v}$ is the velocity vector of gas, X is the extent of reaction, φ is the volumetric molar number of salt contributing to the chemical reaction and M_{H_2O} the molar mass of water.

Momentum conservation

To determine the flow regime, Knudsen number can be used. Four distinct flows can be distinguished regarding this number [6]. Under the conditions of our case, the flow is classified as continuum, meaning the Navier-Stokes equations with no-slip boundary conditions are applicable.

At the beginning of the simulation, the Reynolds number of flow in porous media is high enough to make the flow depict non-Darcian behavior. To account for the effect of the porous mediums on the flow, Brinkman equations are implemented which extends Darcy's law to include viscous transport in the momentum balance. The momentum balance can be linked with the source term of consumption/production steam as below:

$$\begin{aligned}\frac{\rho_g}{\varepsilon}\frac{\partial(\vec{v})}{\partial t} + \frac{\rho_g}{\varepsilon}(\vec{v}.\nabla)\vec{v}\frac{1}{\varepsilon} &= \nabla.\left[-pI + \frac{\mu}{\varepsilon}(\nabla\vec{v} + (\nabla\vec{v})^T) - \frac{2}{3}\frac{\mu}{\varepsilon}(\nabla.\vec{v})I\right] \\ &- \left(\frac{\mu}{\kappa} + \beta\rho_g|\vec{v}| + \frac{\frac{dX}{dt}\varphi M_{H_2O}}{\varepsilon^2}\right)\vec{v}\end{aligned} \tag{6}$$

here, μ is the dynamic viscosity, p is the pressure, κ is the permeability of the porous medium, β is the inertial resistance coefficient based on the Forchheimer parameter.

Energy conservation

It is assumed that there is a local thermal equilibrium between steam and reactive material. The energy balance within the salt domain with respect to the heat source of $\frac{dX}{dt}\varphi\Delta H_R$ is given by:

$$\left(\rho C_p\right)_{eff}\frac{\partial T}{\partial t} + \rho_g C_{p,g}(\vec{v}.\nabla T) - \nabla.\left(k_{eff}\nabla T\right) = -\frac{dX}{dt}\varphi\Delta H_R \tag{7}$$

in which the effective heat capacity for the solid-gas pair is obtained as:

$$\left(\rho C_p\right)_{eff} = \varepsilon\rho_g C_{p,g} + (1 - \varepsilon)\rho_s C_{p,s} \tag{8}$$

where ρ_s and $C_{p,s}$ are the density and heat capacity of salt, respectively. Also, k_{eff}, the effective thermal conductivity is computed as the weighted arithmetic mean of fluid and porous matrix conductivities:

$$k_{eff} = \varepsilon k_g + (1 - \varepsilon) k_s \tag{9}$$

The effect of material porosity variation on transport phenomena and bed properties is reflected in modelling as below:

$$\varepsilon = \varepsilon_a + h(\varepsilon_m - \varepsilon_a) \tag{10}$$

where h is the hydrate level and is equal to *X* for hydration and *1-X* for dehydration, and ε_a and ε_m respectively refer to the porosity of anhydrous and monohydrate salt.

4 Validation

Firstly, the heat transfer by conduction within the reactor and the heat loss through convection were examined. This included analyzing the heat input from the heating cords along with convective losses from all external surfaces, excluding the insulated bottom. In this transient simulation, once the simulated probe temperatures at the thermocouple locations matched the steady-state temperatures recorded before the reaction began, those results were used as the initial condition for the second phase, i.e., the reaction itself. Figure 2a illustrates the placement of the thermocouples. Figure 2b presents the experimental temperature measurements before the onset of the reaction, while Figure 2c depicts the temperature variation during the simulation. In these simulations, it is assumed that the reactor initially is at room temperature, and the heating cords begin supplying heat at 250 °C. After approximately 25 minutes, a balance between heat input and heat loss is achieved, stabilizing the temperature at around ~232 °C.

a)

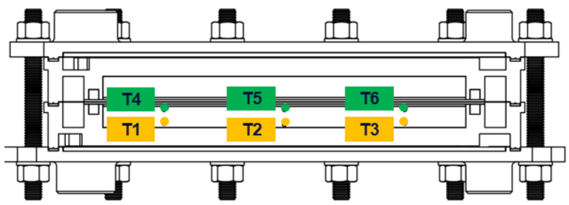

b)

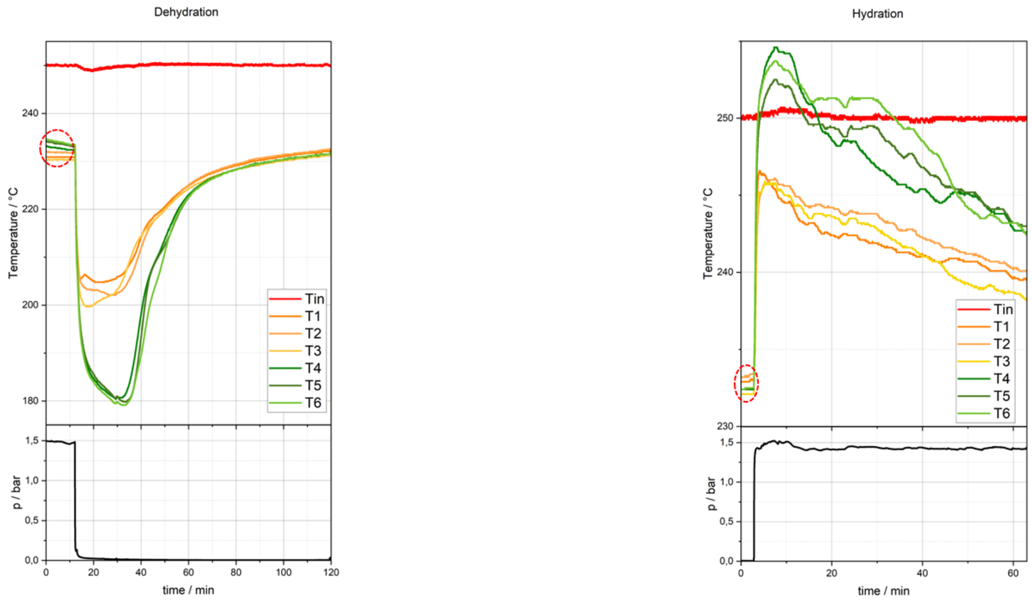

c)

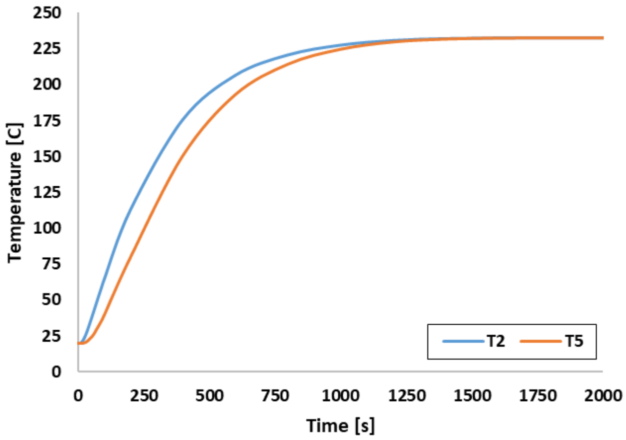

Figure 2. a) Side view of the reactor with the distribution of the thermocouples in the lower material bed; b) Temperature of experiments; c) Temperature of preheating simulation.

The steady-state results from previous transient simulations were used as the initial conditions for this study. The transport phenomena were coupled with reaction kinetics and solved for the system. Figure 3 presents a comparison between experimental measurements and simulation results for hydration at four thermocouple locations: T1, T2, T4, and T5. Overall, the simulation successfully captures the general behavior observed in the experiments. Initially, the reaction proceeds rapidly due to a high reaction rate; however, as the temperature of the reactive material increases and approaches the equilibrium temperature, the reaction rate gradually declines, leading to a continuous decrease in the slope of the conversion curve. As the reaction nears completion, heat conduction from the material to the heat exchanger surfaces surpasses the heat generated by the reaction, causing the overall temperature to decrease.

When comparing simulation results to experimental data, the model predicts the maximum salt temperature at T1 to be 247.6 °C at 250 s; approximately 1 °C higher than the experimental peak, but with a delay of about 3 minutes. For T2, both simulation and experimental results peak at the same time, with temperatures of 248.8 °C and 246.1 °C, respectively. At T5, the simulation reaches a peak of 255.5 °C compared to 252.5 °C experimentally. In contrast, the T4 predictions closely match the experimental data. As the reaction progresses towards completion, discrepancies between the simulation and experiments become more noticeable. This is largely attributed to the increasing influence of heat conduction from the material to the heat exchanger. A detailed discussion regarding the causes of these differences for both the hydration and dehydration stages will be provided later in the next section.

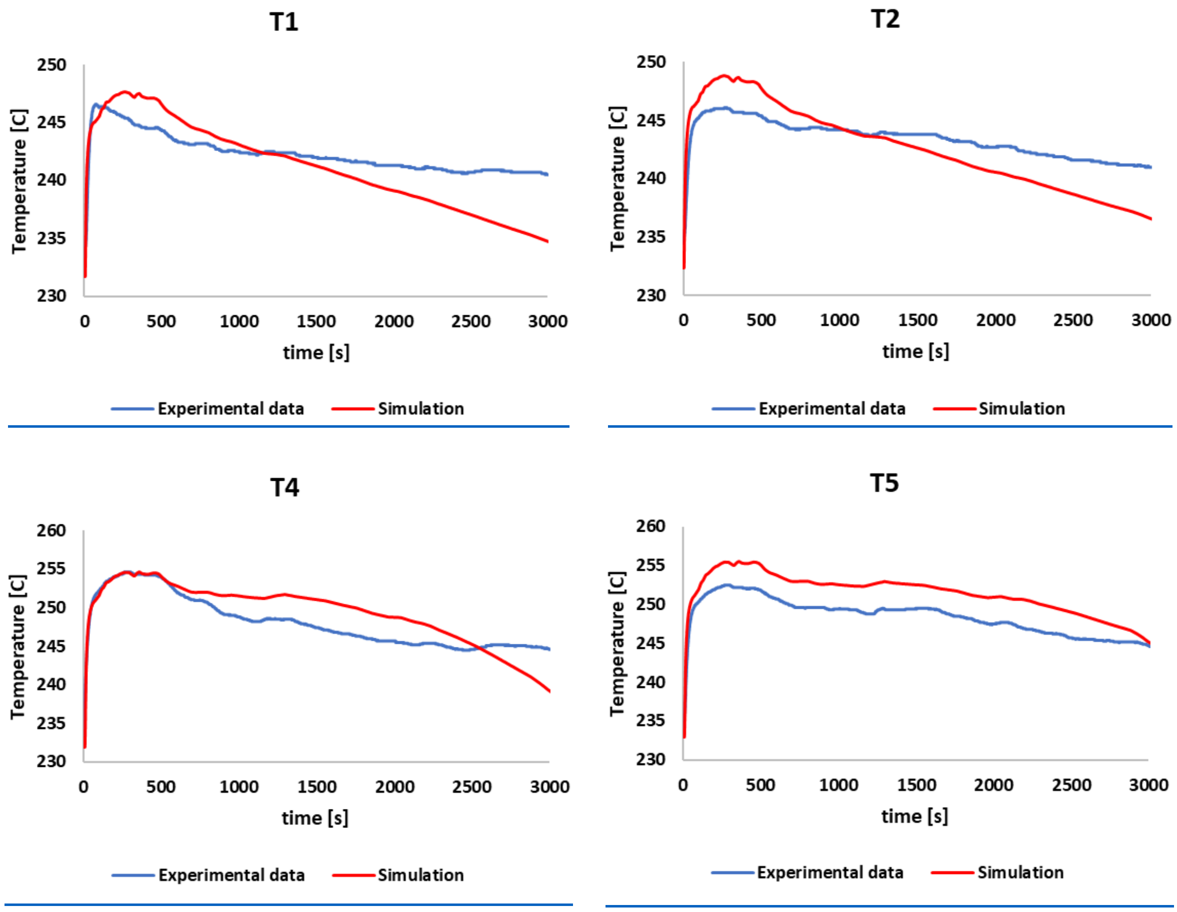

Figure 3. Comparison of experimental and simulated temperature profiles during hydration at different Locations

Figure 4 presents the comparison between simulation results and experimental data for thermocouples T2 and T5 during the dehydration process. As observed, the simulation does not replicate the experimental behavior as accurately as it did during hydration. Initially, material conversion and consequently the temperature change occur rapidly due to a high driving force. However, the simulation predicts a faster temperature drop, reaching lower minimum values earlier than observed experimentally. In contrast, the experimental data show a noticeable delay in the temperature decline, with the material maintaining its minimum temperature for a longer duration at both the lower and upper sensor locations.

In general, the overprediction of the conversion rate by the reaction kinetics model during the initial stage results in a larger thermal sink within the bed, leading to lower simulated temperatures compared to experimental measurements. This deviation propagates into the intermediate stage of dehydration, where the model predicts earlier completion of the reaction relative to the experimental timeline. As a result, an imbalance develops between the heat absorbed by the reactive material and the heat supplied by the heating cords, causing the simulated temperature to increase more rapidly than observed experimentally. Nevertheless, the discrepancies observed from the intermediate stage onward could potentially be mitigated by incorporating the effects of thermal contact resistance arising from the formation of a gap between the material and the aluminum surfaces. Despite numerous parametric studies, uncertainties associated with the early stage of simulations persist, contributing to the remaining disagreements between the model and experimental results.

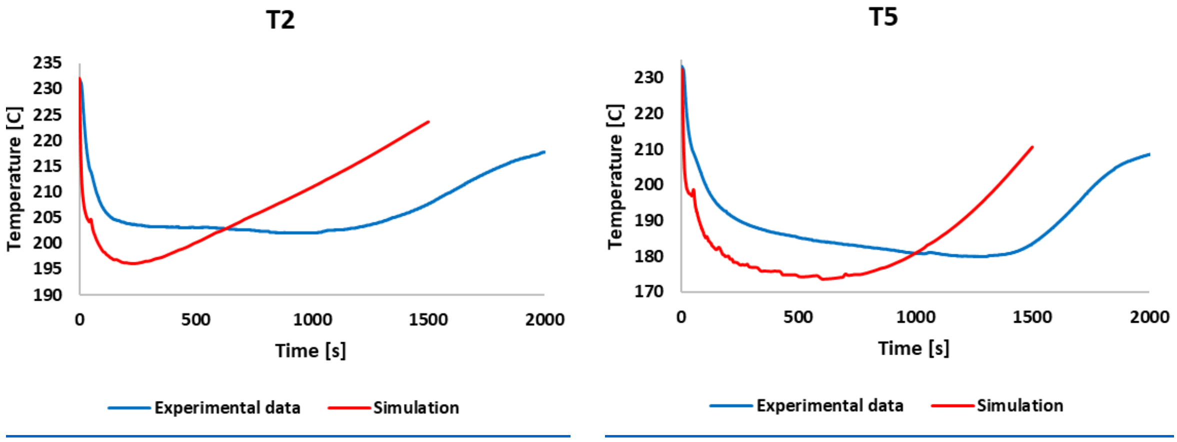

Figure 4. Comparison of experimental and simulated temperature profiles during dehydration at different Locations

5 Discussion and Next Steps

Several sources of uncertainty can be identified during the investigation of the system.

Firstly, although efforts were made during the experiments to maintain the external surface temperature of the reactor at a constant level, unavoidable heat losses occurred. While an attempt was made to develop a representative external heat transfer model, investigation of the preheating phase was beyond the scope of the experimental work. Consequently, external heat transfer was only modeled to match the initial temperature conditions observed in the experimental data, as explained in Figure 2.

Secondly, validation was performed using data from the third cycle, based on discussions with the experimental team. However, it was noted that, after repeated cycles, the powder bed underwent structural changes, transforming into a more compact, brick-like form. This agglomeration likely altered the diffusion characteristics within the bed, leading to delayed activation of certain regions during the reaction compared to the model, which assumes a bed with uniform porosity.

Thirdly, the level of hydration during experiments was not directly measured. As a result, there is uncertainty regarding the actual progression of conversion and whether the material was fully converted at the end of each half-cycle. Specifically, it is unclear whether the entire material was in the monohydrate state at the onset of dehydration and in anhydrous state for the hydration test. In the simulations, it was assumed that full conversion occurred in the preceding half-cycle, leading to a greater amount of reactive material available as a heat source or sink than may have been the case experimentally.

Fourthly, the discrepancies from the intermediate stages onward could potentially be attributed to the growing influence of heat conduction from the material to the heat exchanger over hydration and vice versa over dehydration, as well as possibly within the material itself. Additionally, it is likely that the formation of a thermal gap between the material and the heat exchanger surfaces, which is caused by material shrinkage, poor contact, or separation due to heat exchanger surfaces' bent, contributes to the reduced heat transfer efficiency. Accounting for modeling this gap could improve the prediction of thermal behavior, especially during the later stages of the reaction when conduction becomes the dominant heat transfer mechanism. Finally, potential inaccuracies could have arisen from slight displacements of the thermocouple probes during material loading and reactor assembly, which could have affected the recorded temperature profiles.

Once the next version of the reactor becomes available and demonstrates promising performance during preliminary evaluations, model development for the new system will commence. Following successful validation of the model against experimental data, the optimization phase will be initiated.

6 Conclusion

A numerical model was developed to analyze the reactor that was tested experimentally. The model was designed in two phases, using experimental data as both the initial and boundary conditions. In the first phase, an attempt was made to create a transient model for heat loss from the reactor, where the temperature data from thermocouples were monitored. Once the temperatures stabilized and balanced with the heat supplied by the heating cords, this steady state was used as the initial condition for the second phase of the reaction. The results obtained from the model demonstrated promising agreement with experimental data, particularly for the hydration phase. However, the model did not show satisfactory results for the dehydration process. This discrepancy indicates that further refinement of the model is needed for dehydration. Overall, while the model provides a valuable tool for understanding the reactor's performance, future work will focus on modeling the next version of the reactor.

7 Bibliography

[1] Stengler J, Bürger I, Linder M. Performance analysis of a gas-solid thermochemical energy storage using numerical and experimental methods. Int J Heat Mass Transf 2021;167. https://doi.org/10.1016/j.ijheatmasstransfer.2020.120797.

[2] Humbert G, Sciacovelli A. Design of effective heat transfer structures for performance maximization of a closed thermochemical energy storage reactor through topology optimization. Appl Therm Eng 2024;239. https://doi.org/10.1016/j.applthermaleng.2023.122146.

[3] Li W, Klemeš JJ, Wang Q, Zeng M. Development and characteristics analysis of salt-hydrate based composite sorbent for low-grade thermochemical energy storage. Renew Energy 2020;157:920–40. https://doi.org/10.1016/j.renene.2020.05.062.

[4] Rui J, Luo Y, Wang M, Peng J, She X. Design and performance evaluation of an innovative salt hydrates-based reactor for thermochemical energy storage. J Energy Storage 2022;55. https://doi.org/10.1016/j.est.2022.105799.

[5] Stengler J, Bürger I, Linder M. Thermodynamic and kinetic investigations of the SrBr2 hydration and dehydration reactions for thermochemical energy storage and heat transformation. Appl Energy 2020;277. https://doi.org/10.1016/j.apenergy.2020.115432.

[6] Karniadakis G, Beskok A, Aluru N. Microflows and Nanoflows: Fundamentals and Simulation. n.d.

CONTACT US

techupgrade.eu

FOLLOW US

Funded by
the European Union

This project has received funding from European Union's Horizon Europe's Research and Innovation Program under grant agreement No. 101103966. Views and opinions expressed are however those of the author(s) only and do not necessarily reflect those of the European Union or the European Climate, Infrastructure and Environment Executive Agency (CINEA). Neither the European Union nor the granting authority can be held responsible for them.